Corrosion Behavior of AISI 409Nb Stainless Steel Manufactured by Powder Metallurgy Exposed in H_2SO_4 and NaCl Solutions

Cabral-Miramontes J. A.[1], Barceinas-Sánchez J. D. O.[2], Poblano-Salas C. A.[3], Pedraza-Basulto G. K.[5], Nieves-Mendoza D.[4], Zambrano-Robledo P. C.[1], Almeraya-Calderón F.[1], Chacón-Nava J. G[5].

[1]Universidad Autónoma de Nuevo León UANL. Facultad de Ingeniería Mecánica y Eléctrica FIME. Centro de Investigación e Innovación en Ingeniería Aeronáutica CIIIA. Carretera a Salinas Victoria Km. 23. Apodaca, Nuevo León. México.
[2] Centro de Investigación en Ciencia Aplicada y Tecnología Avanzada (IPN) Cerro Blanco 141, Colinas del Cimatario 76090, Querétaro, Qro., México.
[3] Centro de Tecnología Avanzada A.C., Procesos de Manufactura, Av. Manantiales 23-A, Parque Industrial Bernardo Quintana, El Marqués Qro. México.
[4] Universidad Veracruzana, Facultad de Ingeniería Civil-Xalapa. Circuito Gonzalo Aguirre Beltrán s/n. Zona Universitaria 91090, Xalapa, Veracruz, México.
[5] Centro de Investigación en Materiales Avanzados, S. C. Departamento de Integridad y Diseño de Materiales Compuestos. Miguel de Cervantes 120, Complejo Industrial Chihuahua 31109. Chihuahua, Chih., México.
*E-mail: josecabral.miramontes80@gmail.com

Powder metallurgy is an effective method for manufacturing stainless steel parts of high quality and accuracy at low cost. However, the use of sintered stainless steels is limited due to their low density, which deteriorates their corrosion resistance. The aim of this study was to determine the corrosion behavior of AISI 409Nb stainless steel specimens sintered with different contents of boron in a hydrogen atmosphere. Boron was added for promoting the formation of a liquid phase during sintering at 1150 °C, thereby achieving a reduction of porosity and increase in density, which is necessary to improve corrosion resistance. The electrochemical techniques of linear polarization resistance (LPR) and electrochemical noise (EN) were used to determine the corrosion behavior of samples with and without additions of boron after immersion in two solutions, 0.5M H_2SO_4 and 0.5M NaCl. The corrosion rates and the possible corrosion mechanisms in the sintered samples were determined. The results indicate that the samples with boron additions are more prone to corrosion due to chromium carbide precipitation.

1. INTRODUCTION

The main attraction of powder metallurgy (PM) is its ability to manufacture stainless steel parts of high quality and practically of any geometry. Parts manufactured by PM can have tight tolerances, and their production costs are lower than those produced by conventional processes. This makes stainless steel PM parts represent a major and growing segment [1, 2]. However, their applications are limited due to their mechanical properties and corrosion resistance, relatively low when compared with wrought and forged products [3, 4]. The properties of sintered products may be higher when the sintering is performed in the presence of a liquid phase rather than in solid state due to an enhanced diffusivity of atoms, which promotes a high densification [3]. The addition of boron to stainless steel powders promotes the formation of a liquid phase and lowers the sintering temperature [5, 6]. The binary phase diagram Fe-B shows the existence of an intermetallic Fe_2B, which forms a eutectic with iron at 1174 ° C, when the boron content is about 4 weight percent [7-9]. The lower corrosion resistance of sintered stainless steels can be attributed to: low density that facilitates the penetration of the electrolyte through the open and interconnected porosity, thereby increasing the active surface; high content of interstitial elements; and formation of intermetallic compounds during sintering [10, 11]. This behavior has been observed in sintered stainless steels that have a microstructure which consists of austenite, ferrite, or combination of these (duplex) despite having a high chromium content [4, 12].

The electrochemical techniques of linear polarization resistance (LPR) and electrochemical noise (EN) have been used to determine the corrosion rate [13, 14] and the type of corrosion occurring in sintered materials [15, 16], respectively.

Thus, in this investigation, the electrochemical behavior of an AISI 409Nb ferritic stainless steel, manufactured by PM, exposed to two solutions, and the effect of boron content on the corrosion behavior were determined.

2. EXPERIMENTAL PROCEDURE

Powders of stainless steel AISI 409Nb, supplied by Coldstream, Ath, Belgium, iron-chromium (Fe-Cr) and iron-boron (Fe-B), supplied by F. W. Winter & Co., Camden, N.J., were used as raw materials. The chemical composition and physical properties of these powders are shown in Table 1. Five mixtures were prepared in which the content of boron was varied from 0.8 to 1.2 weight percent; a reference sample with no addition of boron was also prepared. Each mixture was doped with iron-chromium (2.6 wt %) in order to increase corrosion resistance of the stainless steel because of possible reactions between chromium and boron.

For comparison purposes, an AISI 409 stainless steel sample was made by melting and casting. The chemical composition and nomenclature of the cast sample (Fe409) and mixtures with different contents of boron are presented in Table 2.

Table 1. Chemical composition and physical properties of the powders.

Powder	Composition (weight %)							Apparent density	Flow
	Fe	Cr	B	C	S	Nb	Si	(g/cm^3)	s/50g
409Nb	87.52	10.9	----	0.01	0.01	0.53	0.9	3.06	26.2
Fe-Cr	24.93	74.0	----	0.03	0.02	----	1.0	4.11	----
Fe-B	79.67	----	18.98	0.35	0.005	----	0.82	1.44	----
Powder	Granulometry (%)								
	-60+80	-80+100	-100+150	-150+200	-200+250	-250+325	-325		
409Nb	0.03	0.19	7.26	31.92	11.99	24.65	23.96		
Fe-Cr	100	----	----	----	----	----	15 max		
Fe-B	----	----	----	----	----	0.01	99.99		

Table 2. Chemical composition and nomenclature of the mixtures.

Mixture	Element content (wt%)						
	Fe	Cr	B	C	S	Nb	Si
Fe409	Bal	12.5	0.0	0.08	0.01	0.48	0.70
Fe0.0B	Bal	13.5	0.0	0.02	0.01	0.50	0.89
Fe0.8B	Bal	13.5	0.8	0.184	0.01	0.47	0.89
Fe0.9B	Bal	13.5	0.9	0.207	0.01	0.47	0.89
Fe1.0B	Bal	13.5	1.0	0.230	0.01	0.46	0.89
Fe1.1B	Bal	13.5	1.1	0.252	0.01	0.46	0.89
Fe1.2B	Bal	13.5	1.2	0.275	0.01	0.46	0.89

The raw powders were blended in a double cone mixer spinning at 20 rpm for 30 min. All mixtures were added with 1 wt% of zinc stearate (Blachford), which acts as a lubricant. Samples were compacted under a pressure of 700 MPa. Sintering was carried out in a horizontal tube furnace at 1150 ºC during 60 minutes in a hydrogen atmosphere, at a heating rate of 20 ºC/min.

A piece of copper wire was attached to the samples before the electrochemical tests. Afterwards, the samples were mounted in resin and ground with emery paper up to 1200 grit size. The electrochemical tests were carried out using a Gill-8 ACM Instruments potentiostat/galvanostat/ZRA employing H_2SO_4 and NaCl deaerated solutions, the concentration of both being 0.5 M. Measurements of linear polarization resistance (LPR) were conducted using an electrode of saturated calomel as reference, a working electrode (samples and Fe409) and a platinum wire that acts as a counter electrode. The linear polarization resistance was measured according to the ASTM G59-97standard [17], with operating parameters of ± 20 mV with respect to the corrosion potential (E_{corr}), and a scan rate of 10 mV/min. From LPR data the corrosion rate was calculated in terms of the corrosion current density, i_{corr}, using the Stern and Geary equation [18], which is presented below:

$$i_{corr} = \frac{26}{LPR} \tag{1}$$

where 26 is the Tafel constant and LPR is the linear polarization resistance. The corrosion rate, expressed in millimeters per year, was calculated in accordance with ASTM G102-89 [19]; this calculation was done according to Equation 2.

$$\text{corrosion rate} = \frac{C\omega i_{corr}}{\rho} \tag{2}$$

where C is a conversion factor (3.27 mm·g/mA·cm·year), ω is the equivalent weight (g), ρ is the material density (g/cm^3), and i$_{corr}$ is the corrosion current density (mA/cm^2).

Electrochemical noise tests, measuring potential and current, were carried out on all polished samples in the two test solutions. With these data the electrochemical noise resistance was determined for all the mixtures according to the ASTM G199-09 standard [20]. For these tests an array consisting of a working electrode (samples and Fe409), a second working electrode (platinum) and a reference electrode of saturated calomel (SCE) was used. The potential and current signals were acquired simultaneously every 1 second for a period of 2048 seconds.

3. RESULTS AND DISCUSSION

3.1. Density

The addition of boron improves densification of the stainless steel AISI 409Nb due to the formation of a boron-rich liquid on grain boundaries during sintering at 1150 ° C, which promotes re-arrangement of particles, solution and reprecipitation of intermetallics, reduction of porosity and grain growth [21]. It has been reported that sintered compact density increases as the boron content increases, which was attributed to the homogenization of the microstructure and grain growth [22]. The formation of borides and occurrence of eutectic reactions between boron and 409Nb stainless steel, below their melting points, are due to the high diffusivity of the former in the α iron phase and carbon content [23, 24].

3.2. Linear polarization resistance

Table 3 shows the test results of linear polarization resistance. The corrosion current density of the samples tested in the 0.5M H$_2$SO$_4$solution remains in the same order of magnitude and the corrosion rate is practically the same. Meanwhile, the Fe409 sample has a corrosion current density of an order of magnitude smaller; therefore its corrosion rate is lower.

Crevice corrosion is the most feasible mechanism that explains the high corrosion rate in sintered steels immersed in a 0.5M H$_2$SO$_4$ solution. The attack begins in the pores, but as the immersion time is prolonged [25], this becomes more aggressive because it moves toward the inside of

the material. Nucleation and propagation of crevices are associated with the creation and development of localized solutions inside cavities and pores. The presence of porosity favors a differential aeration in crevices and a differential concentration of protons. Under these conditions, the corrosion potential of aerated zones of a crevice is greater than the passivation potential, thus the passive layer remains stable. In contrast, when there are active conditions inside the pores, active-passive cells are created. The onset of crevice corrosion in sintered materials is produced through the enrichment of metal ions, mainly chromium, inside the pores, which leads to acidification as a result of the hydrolysis reaction $Cr^{3+} + 3H_2O \leftrightarrow Cr(OH)_3 + 3H^+$ [26].

The corrosion current density and corrosion rate measured in the samples immersed in the NaCl 0.5 M solution were smaller than the values measured in the sulfuric acid solution. The corrosion rate for the majority of the samples was in the same order of magnitude. In this case, the presence of chloride has a significant effect on the stability of the passive layer. Corrosion by pitting in passive metals is eased by the existence of weak sites (defects and pores) in the oxide layer. In duplex and martensitic stainless steels pitting occurs in the open porosity and tends to propagate towards the inside of the material [4, 27]. This mechanism may occur in several samples analyzed in this investigation. In these materials, crevice corrosion can result from depletion of the dissolved oxygen in the pore. Oxygen deficiency impairs the passive layer and produces an accumulation of metal cations within the pore. An increase in the concentration of cations induces a flow of chloride ions into the pores to balance the charges. The high concentration of chlorides and occurrence of acidic hydrolysis reactions within the pores can produce localized metal dissolution [11].

Table 3. Electrochemical parameters and corrosion rates derived from the Linear Polarization Resistance method.

Sample	Solution	E_{corr}, (mV vs. ECS)	LPR, Ω-cm^2	i_{corr}, mA/cm^2	Corrosion rate, mm/year
Fe409	0.5M H$_2$SO$_4$	-535.0	49.32	0.52	5.87
Fe0.0B		-538.2	10.85	2.39	29.30
Fe0.8B		-478.9	8.97	2.89	36.05
Fe0.9B		-478.9	9.69	2.68	33.33
Fe1.0B		-476.1	9.49	2.73	31.95
Fe1.1B		-470.3	9.40	2.76	32.02
Fe1.2B		-470.7	9.10	2.85	32.83
Fe409	0.5M NaCl	-569.8	529.39	0.049	0.547
Fe0.0B		-489.3	3252.66	0.007	0.097
Fe0.8B		-580.9	961.74	0.027	0.336
Fe0.9B		-563.1	963.43	0.026	0.335
Fe1.0B		-600	584.14	0.044	0.519
Fe1.1B		-609.6	583.02	0.044	0.515
Fe1.2B		-630.2	706.96	0.036	0.422

3.3. Electrochemical noise (EN)

Electrochemical noise determination is characterized by measuring stochastic fluctuations of current and potential without externally perturbing the original conditions of the system [28]. In the present work, the current and potential system noise signals were refined by employing a fifth degree polynomial model; the magnitude of noise was calculated by employing the residuals [29].
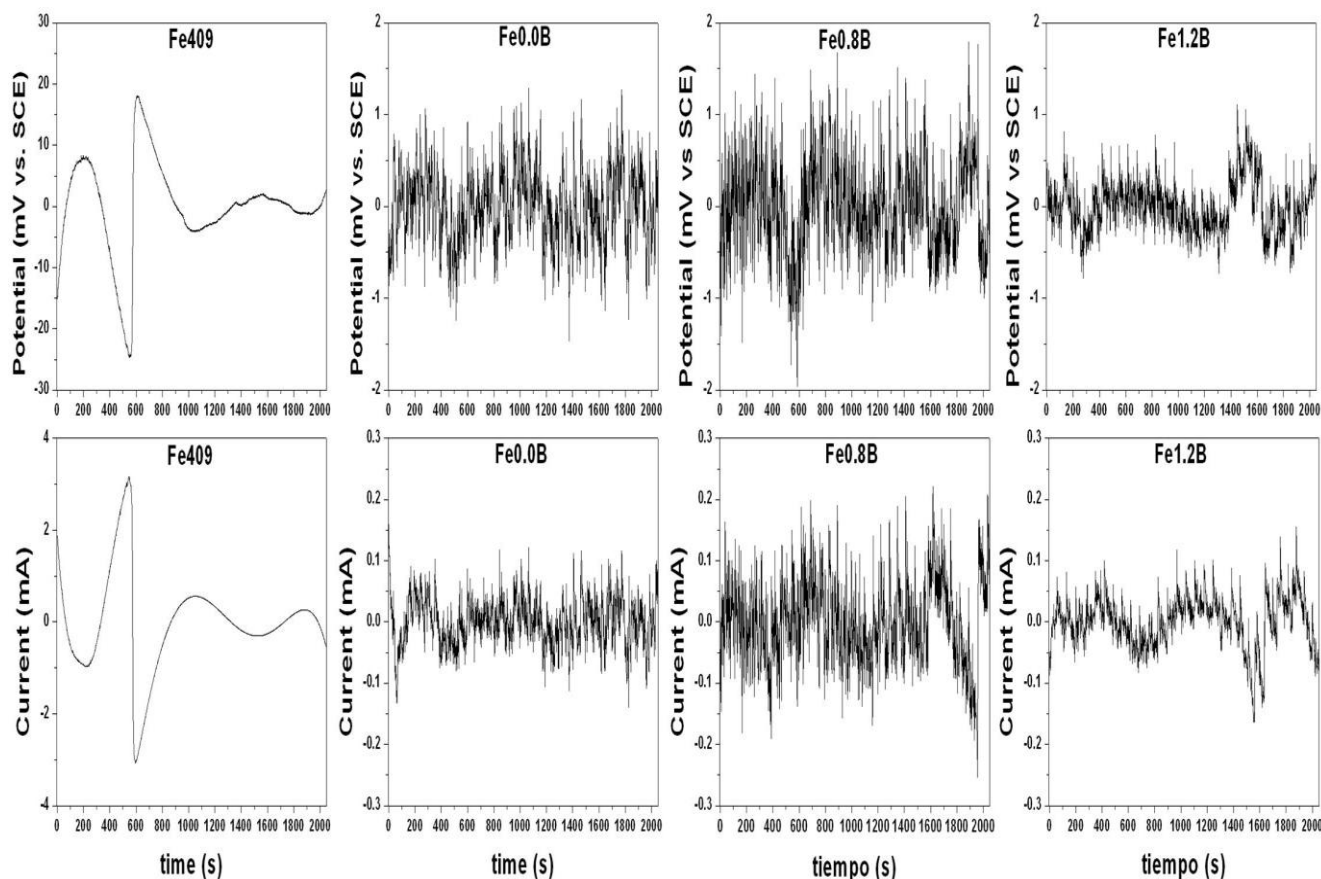
Figure 1 shows potential and current time series with tendency for samples tested in a 0.5 M H_2SO_4 solution. It can be seen that the bulk sample does not show pronounced fluctuations in potential and reach a constant behavior, which indicates that the surface tends to passivate in this solution. This behavior is also reinforced by looking to the current fluctuations, in which a decreasing tendency was observed followed by a constant trend at longer testing times. Such behavior suggests that the surface suffers passivation, since a constant current is measured in the system as immersion time increases [30]. Conversely, powder metallurgy samples show more active potentials with higher currents as testing time increases, with all samples showing comparable current levels. Also, they showed larger current and potential fluctuations than bulk counterparts.
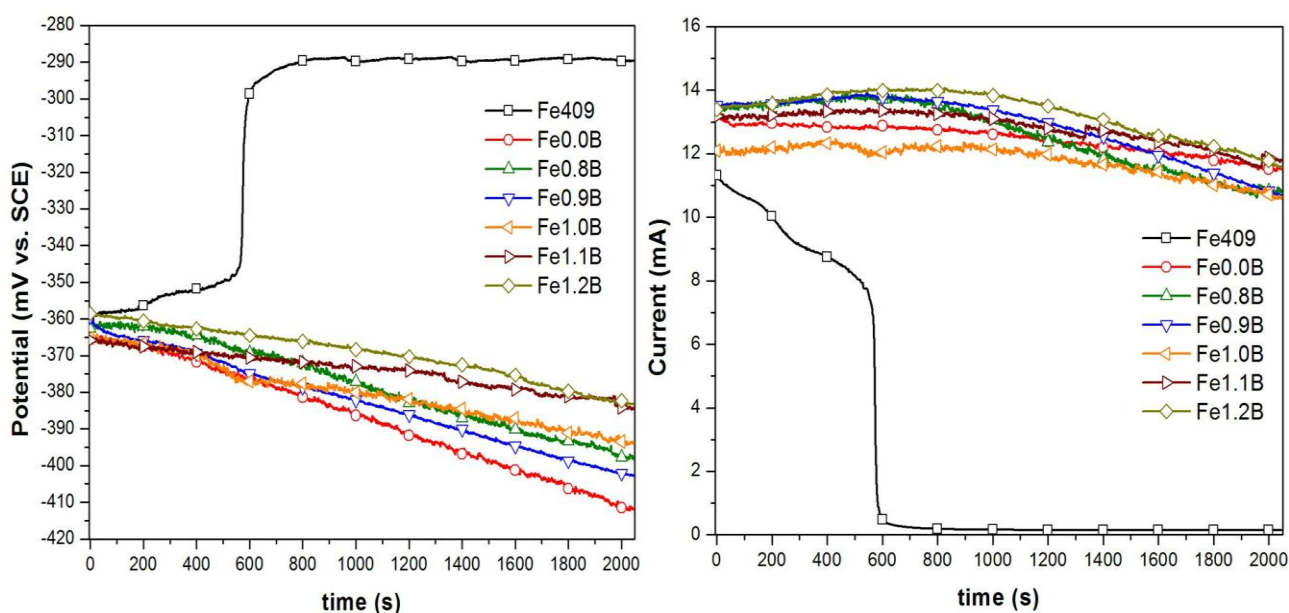
Figure 1. Potential and current time records without trend removal for samples exposed in 0.5M H_2SO_4 solution.

Figure 2 shows potential and current time series without tendency for samples Fe409, Fe0.0B, Fe0.8B and Fe1.2B, all immersed in a 0.5M H_2SO_4 solution. Potential fluctuations of sample Fe409 are an order of magnitude larger than those of the three other samples. Also, noise signal from sample Fe409 contains low frequency and high amplitude fluctuations. Those fluctuations decrease as testing time increases, suggesting the occurrence of passivation of the surface. On the other hand, PM samples show low amplitude-high frequency fluctuations, both in current and also in potential, which are characteristic features of uniform corrosion phenomena occurring on those samples. Fluctuations in PM samples can also arise from electrolyte penetration or air entrapment within the pores network

[31]; they also can be produced from nucleation of hydrogen bubbles during active dissolution in acid media [32]. All samples were studied by optical microscopy after electrochemical noise testing in the H₂SO₄ solution. PM samples showed a more pronounced electrochemical attack at inter-particle boundaries than the bulk counterparts (see Figure 5).

Figure 2. Potential and current time records without trend removal for samples Fe409, Fe0.0B, Fe0.8B and Fe1.2B exposed in 0.5M H₂SO₄ solution.

Potential and current vs. time data, with tendency, for samples tested in the NaCl solution are shown in Figure 3. All samples tested show active corrosion potentials as testing time proceeds, with more active values for PM specimens; except for sample Fe0.0B which showed stable corrosion potential values around -450 mV. Bulk Fe409 sample showed potential fluctuations as testing time increased, reaching a maximum of -400 mV between 1200 to 1600 s, the same fluctuations were also observed for current density measurements. Current density trend was similar for all PM samples, with sample Fe1.2B showing the highest current density. In general, for PM samples, those with higher boron contents showed higher current densities. Bulk and PM samples showed localized corrosion when tested in a 0.5M NaCl solution; in the first case the mechanism may occur as the passive layer is broken by the chloride ions within the solution, which in turn generates a very large cathodic/anodic surface ratio [33]. In PM samples the presence of pores is the most important factor leading to the occurrence of localized corrosion, which masks any influence of the microstructure or chemical

composition on corrosion behavior. Finally, corrosion of PM samples in NaCl can be attributed to electrolyte penetration into the pores network and also to air entrapment within the same network.
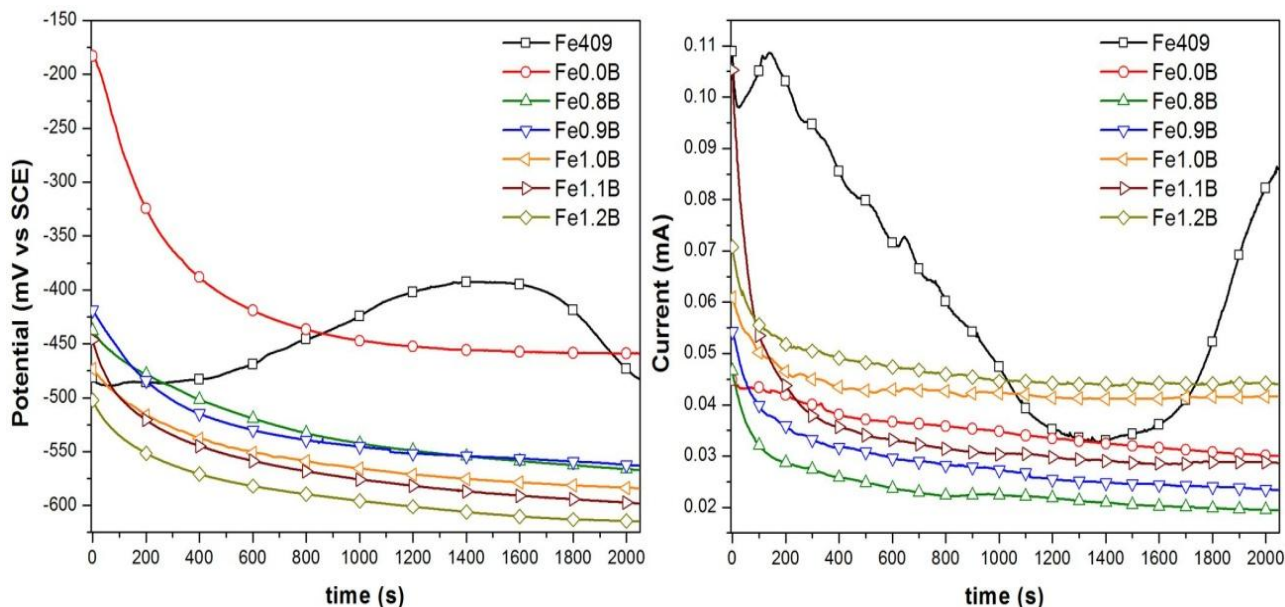
Figure 3. Potential and current time records without trend removal for all samples exposed in 0.5M NaCl solution.

Figure 4 shows the potential and current versus time series, with tendency removal, for samples Fe409, Fe0.0B, Fe0.8B and Fe1.2B tested in a 0.5M NaCl solution. Samples Fe409 and Fe0.0B presented similar fluctuations in potential which were higher than those measured in samples Fe0.8B and Fe1.2B. On the other hand, current fluctuations for sample Fe409 were significantly higher than those from specimens Fe0.0B, Fe0.8B and Fe1.2B, whose current variations fell within +/- 0.002 mA. For all samples, the anodic transients were high at the beginning of the test, followed by a decreasing tendency and further stabilization around +/-0.001 mA, as testing time proceeded. This suggests the occurrence of localized corrosion phenomena in the samples [31]. This form of corrosion promotes transient electrochemical noise signals, as the superficial and sub-superficial cavities hinder ion diffusion; and is promoted by a mechanism which is similar to that of pitting caused by chloride ions [34]. The main difference is that crevice corrosion prevails for longer times than pitting; such a behavior was observed here in PM samples. Noise transients for crevice corrosion in stainless steel are similar to those produced by a stable pit, lasting several hours [35].

In PM samples, porosity acts as a reservoir for chloride ions. Interparticle friction during sintering is an important factor that contributes to localized corrosion at the particle-pore interface. During sintering, friction of particle surface promotes localized abrasion and consequently, during immersion in a corrosive media, instability of the passive layer in those zones. Such a layer may not be able to regenerate due to the low oxygen partial pressure at that constricted regions. Therefore, if particle bonding is not completed during sintering, anodic active localized zones are expected to be formed at the pore-particle interfaces. Corrosion in those regions results in partial disintegration of the

sintered structure. Figure 5 shows this phenomenon occurring in samples Fe0.0B and Fe1.2B. Resistance calculated form noise measurements (R_n) can be expressed as the ratio of potential and current standard deviations (σ_E and σ_I) multiplied by the total area (A), as in Ohm´s law [20], see Equation 3.

$$R_n = \frac{\sigma_E A}{\sigma_I} \qquad (3)$$

R_n can be compared to linear polarization resistance measurements, therefore, is possible to calculate corrosion rates by employing equations 1 and 2. The localization index (LI) is commonly employed as a way of measuring corrosion and is expressed as

$$LI = \frac{\sigma_I}{Irms} \qquad (4)$$

Where σ_I and I_{rms} are the standard deviation of the current and root square mean of current fluctuation value, respectively. LI values between 0.1 and 1 indicate localized corrosion, whereas general corrosion is found for 0.001>LI<0.01. Finally, a mixed corrosion mode is found for values between both ranges [36, 37].
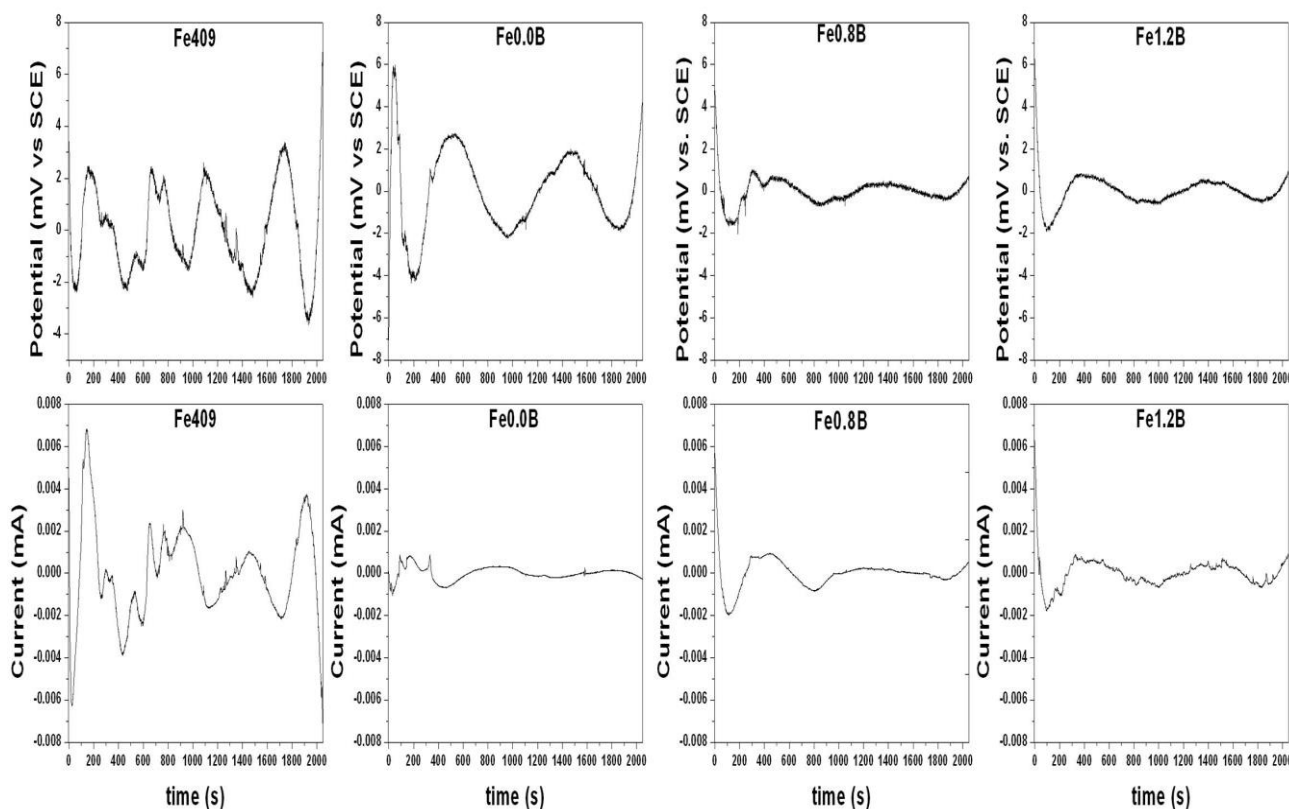
Figure 4. Potential and current time records without trend removal for samples 409, Fe0.0B, Fe0.8B y Fe1.2B exposed in 0.5M NaCl solution.

Table IV shows σ_v, σ_I, R_n and LI values for the whole set of samples studied here. Most of the samples immersed in the NaCl solution showed localized corrosion, whereas corrosion of samples Fe1.0B and Fe1.2B presented a mixed mode. Samples immersed in H_2SO_4 showed mixed corrosion; evidence of localized corrosion was only found in specimen Fe409. Metallographic evidence shown in Figure 5 is in good agreement with the results regarding corrosion type included in Table IV.

Table IV. Electrochemical noise parameters, corrosion rates, LI and corrosion type in both solutions for all specimens.

Sample	Solution	σ_v	σ_I	R_n, $\Omega\text{-cm}^2$	Corrosion rate, mm/year	LI	Corrosion type
Fe409	0.5M H_2SO_4	0.095	9.29E-4	102.620	3.097	0.729	Localized
Fe0.0B		0.412	0.039	10.416	30.52	0.035	Mix
Fe0.8B		0.525	0.070	7.479	43.24	0.082	Mix
Fe0.9B		0.401	0.028	14.329	22.53	0.073	Mix
Fe1.0B		0.837	0.085	9.848	30.79	0.040	Mix
Fe1.1B		0.502	0.082	6.099	49.35	0.039	Mix
Fe1.2B		0.282	0.042	6.651	44.92	0.053	Mix
Fe409	0.5M NaCl	1.700	2.20E-3	775.4	0.373	0.361	Localized
Fe0.0B		1.988	3.13E-4	6167.8	0.051	0.109	Localized
Fe0.8B		0.624	7.24E-4	861.7	0.375	0.184	Localized
Fe0.9B		0.647	5.87E-4	1104.6	0.292	0.188	Localized
Fe1.0B		0.384	3.67E-4	1047.3	0.289	0.074	Mix
Fe1.1B		1.642	2.30E-3	724.6	0.415	0.294	Localized
Fe1.2B		0.725	6.75E-4	1073.5	0.278	0.091	Mix

Figure 6 shows a summary of the calculated corrosion rates for samples immersed in NaCl and H_2SO_4, employing linear polarization resistance and electrochemical noise techniques. Samples tested in H_2SO_4 showed higher corrosion rates than those immersed in NaCl, being such a difference around two orders of magnitude. No evident effect of boron additions on corrosion rate was found. On the other hand, for samples tested in NaCl an increased corrosion rate was observed as the boron content was higher.

For the various alloys tested in H_2SO_4 and NaCl solutions, the corrosion rates measured by electrochemical noise were comparable to those obtained by linear polarization resistance. This suggests that the former technique can be used accurately for measuring corrosion phenomena in samples processed by powder metallurgy.
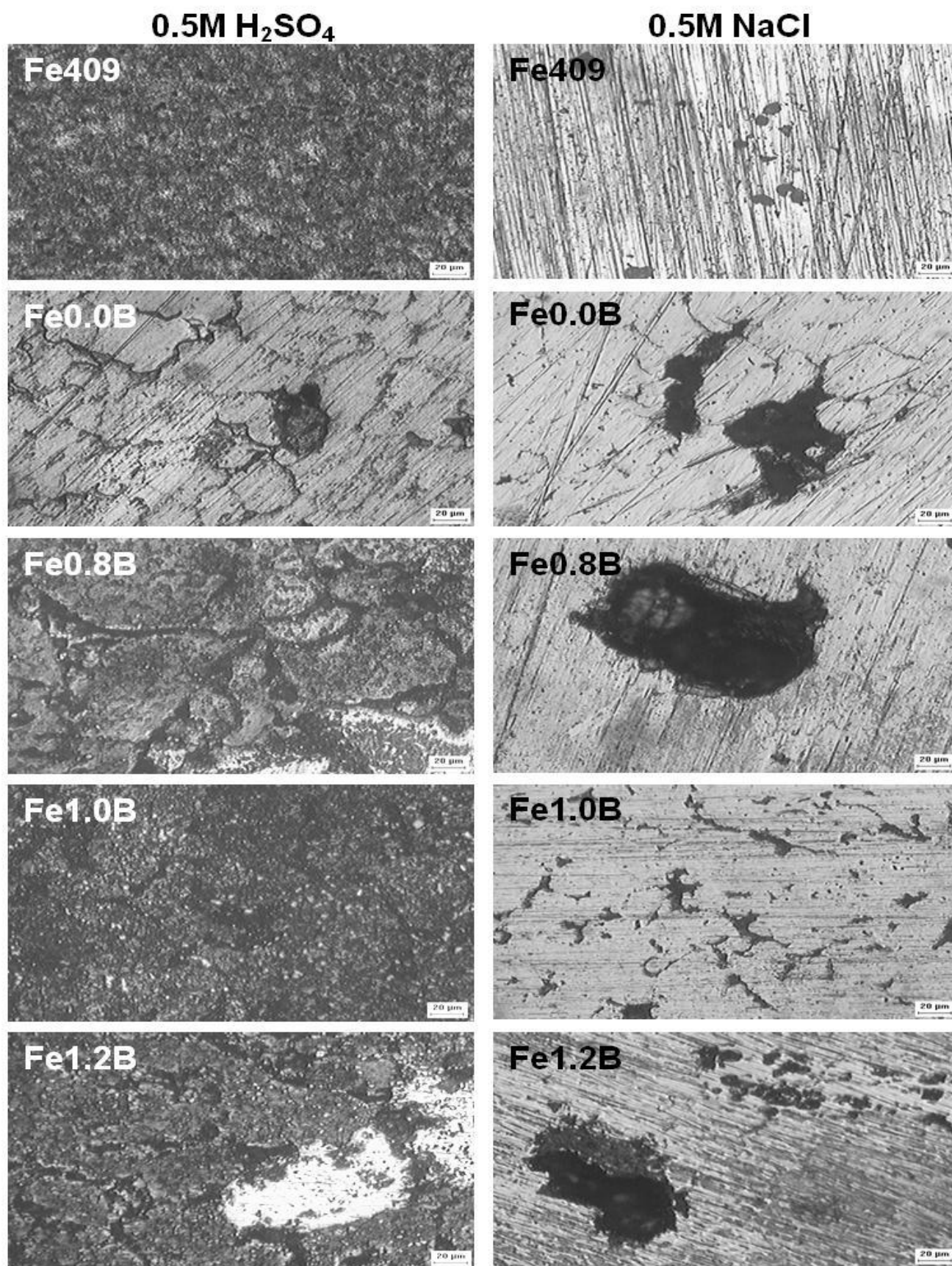
Figure 5. Optical micrographs in plan after electrochemical noise measurements for specimens exposed in 0.5M of H_2SO_4 and 0.5M of NaCl solutions.
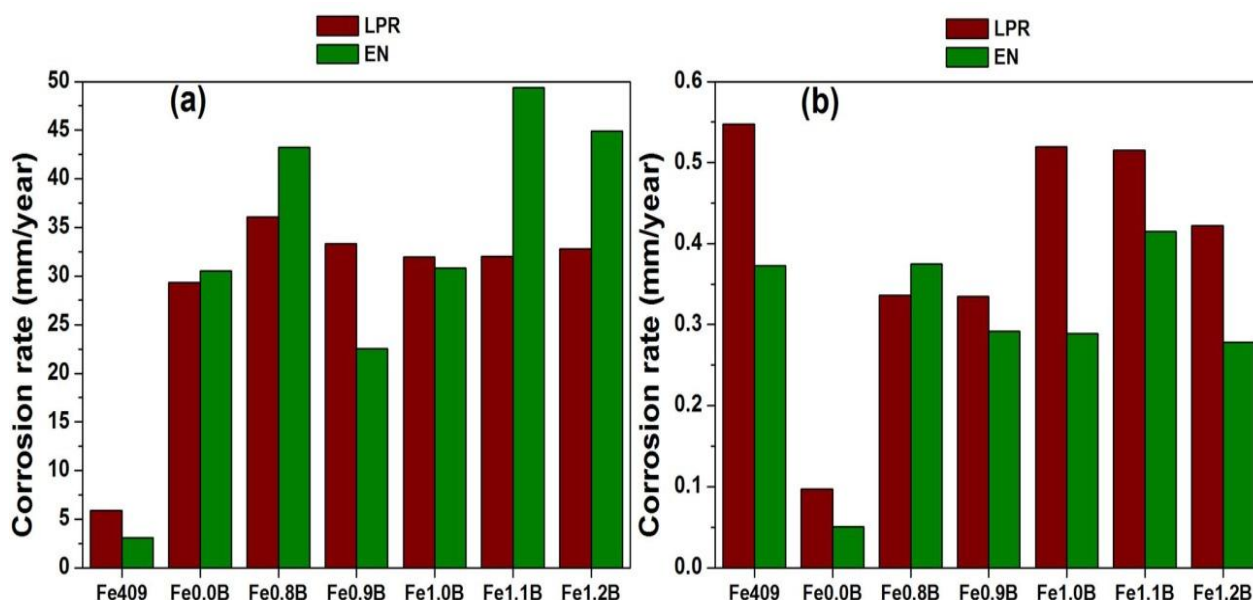
Figure 6. Corrosion rates calculated from linear polarization resistance and electrochemical noise measurements for all samples exposed in a) 0.5M H_2SO_4 solution and b) 0.5 M NaCl solution.

4. CONCLUSIONS

Compacted and sintered steel samples tested in H_2SO_4 solution showed higher corrosion rates than those measured in a NaCl electrolyte. This can be attributed to hydrolysis occurring at the surface of samples, which involves local concentration of protons, that in turn results in dissolution of the passive layer and formation of active-passive cells within the pores. Such mechanism is complemented by a crevice corrosion mechanism.

Sample without boron showed the best corrosion resistance when tested in NaCl, this can be attributed to its lower carbon content, which hinders the formation of carbides that may act as corrosion initiation sites.

Electrochemical noise measurements showed a mixed corrosion mechanism for samples tested in H_2SO_4, whereas samples immersed in NaCl presented degradation by localized corrosion.

Current and potential behavior of samples tested in H_2SO_4 during noise measurements was erratic; this was attributed to electrolyte flow through superficial pores and air displacement from those regions into the solution.

Boron additions are deleterious to PM 409Nb stainless steel corrosion resistance, as B-containing samples showed the highest corrosion rates among the samples studied here.

A good correlation between electrochemical noise and linear polarization resistance measurements was found in this study, which suggests that the former technique is a reliable technique useful for corrosion evaluation of alloys manufactured by PM techniques.

References

1. A. Toro., F.A. Filho., D. Rodrigues., A.P. Tschiptschin. and N.A. Falleiros., *V Congreso Colombiano de Corrosión y Protección*, in *V Congreso Colombiano de Corrosión y Protección*. 1999: Cartagena de Indias, Colombia. p. 51-60.
2. W. Schatt and K.P. Wieters, *Powder Metallurgy: Processing and Materials*. E.P.M.A., Shrewsbury, UK (1997).
3. J. Shankar, A. Upadhyaya and R. Balasubramaniam, Corros. Sci, 46 (2004) 487
4. L.A. Dobrzański, Z. Brytan, M. Actis Grande and M. Rosso, *J. Mater. Process. Tech*, 191 (2007) 161
5. D. Krecar, V. Vassileva, H. Danninger and H. Hutter, *Anal. Bioanal. Chem*, 379 (2004) 605
6. M. Selecká, A. Šalak and H. Danninger, *J. Mater. Process. Tech*, 141 (2003) 379
7. T.B. Sercombe, *Mater. Sci. Eng. A*, 363 (2003) 242
8. M. Sarasola, T. Gómez-Acebo and F. Castro, *Powder Metall*, 48 (2005) 59
9. T.B. Massalski, *Binary Phase Diagrams*. Second edition, A.S.M. International. Vol. 1 and 2., Materials Park, OH. USA (1986).
10. A. Bautista, F. Velasco and J. Abenojar, *Corros. Sci*, 45 (2003) 1343
11. M.C. Baron and B.A. Shaw., NACE, Paper 548 (1998) 1
12. E. Otero, A. Pardo, M.V. Utrilla, E. Sáenz and J.F. Álvarez, *Corros. Sci*, 40 (1998) 1421
13. G. Rocchini, *Corros. Sci*, 38 (1996) 2095
14. J.R. Scully, *Corrosion*, 56 (2000) 199
15. J.U. Chavarín and J. M. Malo, Research trends, *Trends in Corrosion Research*, 2 (1997) 49-58
16. R.A. Cottis, *Corrosion*, 57 (2001) 265-285
17. ASTM-G59, *Standard test method for conducting potentiodynamic polarization resistance measurements*, ASTM International, West Conshohocken, PA (1997).
18. M. Stern and A.L. Geary, *J. Electrochem. Soc*, 104 (1957) 56
19. ASTM-G102, *Standard Practice for Calculation of Corrosion Rates and Related Information from Electrochemical Measurements*, ASTM International, West Conshohocken, PA. (1999).
20. ASTM-G199,*Standard guide for electrochemical noise measurement*, ASTM International, West Conshohocken, PA. (2009).
21. R.M. German, *Liquid phase sintering*. Plenum Press, New York, EE UU. (1985).
22. J. Cabral Miramontes, J. Barceinas Sánchez, F. Almeraya Calderón, A. Martínez Villafañe and J. Chacón Nava, *J. Mater. Eng. Perform*, 19 (2010) 880
23. J.A. Cabral-Miramontes, J.D.O. Barceinas-Sánchez, L. Vélez-Jacobo, A. Martínez-Villafañe y J.G. Chacón-Nava, *Rev. Metal. Madrid*, 44 (2008) 493
24. J.A. Cabral Miramontes, Ph D. Thesis. Centro de Investigación en Materiales Avanzados. Chihuahua, Chih, México. (2010)
25. C. Padmavathi, A. Upadhyaya and D. Agrawal, *Scripta Mater*, 57 (2007) 651
26. E. Otero, A. Pardo, M.V. Utrilla, F.J. Pérez and C. Merino, *Corros. Sci*, 39 (1997) 453
27. C. P. Castillo-Morquecho, C. Lopez-Melendez, M. I. Flores-Zamora, R. G. Bautista-Margulis, H. E. Esparza-Ponce, F. Almeraya-Calderón, C. Gaona-Tiburcio, A. Martínez-Villafañe, *Int. J. Electrochem. Sci.* 7 (2012) 1125
28. R. A. Cottis and S. Turgoose, Corrosion Testing Made Easy, (1999)

29. D.L. Reichert, *Electrochemical noise measurement for determining corrosion rates*, ASTM STP 1277 (1996) 79
30. F. Almeraya-Calderón, F. Estupiñán-Lopez , P. Zambrano-Robledo, A. Martínez-Villafañe, A. Borunda-Terrazas, R. Colás-Ortiz y C. Gaona-Tiburcio, *Rev. Metal. Madrid*, 48 (2012) 147
31. S. Balaji, G. Joshi and A. Upadhyaya, *Scripta Mater*, 56 (2007) 149
32. J.L. Dawson, *Electrochemical noise measurement: The definitive In Situ technique for corrosion applications?*, American Society for Testing and Materials, (1996) 3
33. E. Otero, A. Pardo, M.V. Utrilla, E. Sáenz and F.J. Perez, *Mater. Charact*, 35 (1995) 145
34. D.A. Jones, *Principles and Prevention of Corrosion*. New York, EE.UU. Maxwell Macmillan International Editions. (1992).
35. A.M.P. Simoes and M.G.S. Ferreira, 10th International Congress on Metal Corrosion. Madras, India. (1987) 3125.
36. D.A. Eden and A. N. Rothwell., *Electrochemical noise data: analysis, interpretation, and presentation*, in Corrosion NACE., Houston, TX. (1992)
37. S. Webster, L. Nathanson, A. G. Green and B.V. Johnson, T*he use of electrochemical noise to asses inhibitor film stability*, in Corrosion NACE, Manchester, U. K. (1992).